G. REACTION MECHANISM STUDIES

Direct Reactions have played a pivotal role in understanding nuclear wavefunctions, residual interactions between nucleons, and collective correlation of particles. Historically, light ion transfers like the (d,p) reaction, were used on stable targets to investigate the structure of states. However, using radioactive beams, reactions in inverse kinematics, and sophisticated detector arrays, the possibility of performing direct reactions on unstable nuclei has emerged. This seems to be a technique with great potential for the future, both at ANL using "in-flight" production of radioactive beams, and at other radioactive beam facilities. In these reactions, and in the studies of far-sub-barrier fusion, improvements in experimental techniques have led to new insights.

g.1. Study of ^{7}He Using the d(^{6}He,p)^{7}He Reaction

(K. E. Rehm, J. P. Greene, D. J. Henderson, R. V. F. Janssens, C. L. Jiang, E. F. Moore, R. C. Pardo, S. C. Pieper, G. Savard, J. P. Schiffer, D. Peterson, S. Sinha, X. Tang, R. B. Wiringa, A. H. Wuosmaa,* L. Jisonna,† M. Paul,‡ and R. E. Segel†)

We have studied the $d(^{6}\mathrm{He},p)^{7}\mathrm{He}$ reaction using a ^{6}He beam to study the properties of the exotic, neutron-rich nucleus ^{7}He. The nucleus ^{7}He, which possesses no particle-bound states, is one of the simplest nuclei for which there remains considerable debate about its structure. The structure of ^{7}He is particularly interesting in light of the current interest in systems containing many loosely bound neutrons. In addition to the well established ground state,[1] several experimental efforts have been made to understand the properties of possible excited states of this system.[2-4] In one of these[4] it has been suggested that there may exist a low-lying level that possesses significant overlap with $^{6}\mathrm{He}_{\mathrm{g.s.}}$ + n, and should thus be populated strongly in the $d(^{6}\mathrm{He},p)^{7}\mathrm{He}$ reaction.

To examine the properties of possible low-lying excited states in this nucleus, we have studied the inverse-kinematic reaction $d(^{6}\mathrm{He},p)^{7}\mathrm{He}$ using a radioactive ^{6}He beam produced at the in-flight facility at the ATLAS accelerator at Argonne National Laboratory. The ^{6}He beam was produced using the $d(^{7}\mathrm{Li},^{6}\mathrm{He})^{3}\mathrm{He}$ reaction, with a primary ^{7}Li intensity of 50 pnA, and primary beam energy of 81 MeV. The resulting ^{6}He secondary beam had an intensity of between 10 and 15 $\times$ 10^{4} particles per second and an energy of 69 MeV. The ^{6}He beam bombarded a 540 μg/cm^{2} thick CD_2 target.

In inverse kinematics at the present bombarding energies, the protons of interest are emitted at backward angles in the laboratory. These protons were detected using an array of segmented annular silicon detectors, and coincident ^{4,6}He ions were detected and identified using an array of silicon EΔE telescopes at very forward angles. Figure I-49 shows a representative Q-value spectrum, obtained for p-^{6}He coincidence events. The ground state is clearly strongly excited, and there also appears a broad distribution of counts that extends to higher excitation energies. The low-lying state reported in[4] lies at an excitation energy of 0.56 MeV, and would therefore appear almost exactly in the valley between the ground state and this broad distribution. If such a state exists, it is not strongly populated in $d(^{6}\mathrm{He},p)^{7}\mathrm{He}$, and is likely not to correspond to a $J^{\pi} = 1/2^{-}$ state as claimed in Ref. 4.

The angular distribution for the $d(^{6}\mathrm{He},p)^{7}\mathrm{He}$ ground-state transition appears in Fig. I-50. Also plotted in Fig. I-50 is a curve representing a calculation of that angular distribution using the code PTOLEMY, taking as input the one-neutron spectroscopic overlap taken from Quantum Monte-Carlo methods. The calculated angular distribution is in reasonable agreement with the data, although the calculation over-predicts the data.

These results have been accepted for publication in Physical Review Letters.

*Western Michigan University, †Northwestern University, ‡Hebrew University, Jerusalem, Israel.

[1] R. H. Stokes and P. G. Young, Phys. Rev. **178**, 2024 (1969).
[2] A. A. Kosheninnikov *et al*., Phys. Rev. Lett. **82**, 3581 (1999).
[3] H. G. Bohlen *et al*., Phys. Rev. C **64**, 024312 (2001).
[4] M. Meister *et al*., Phys. Rev. Lett. **88**, 102501 (2002).

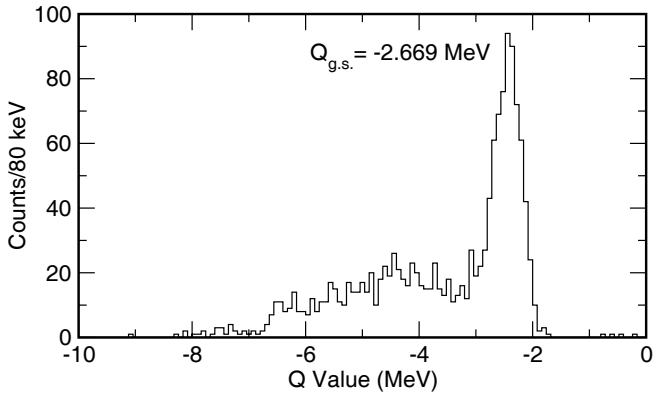

Fig. I-49. Proton Q-Value spectrum from the d(^{6}He,p)^{7}He reaction for $110^o \leq \theta_p \leq 160^o$.

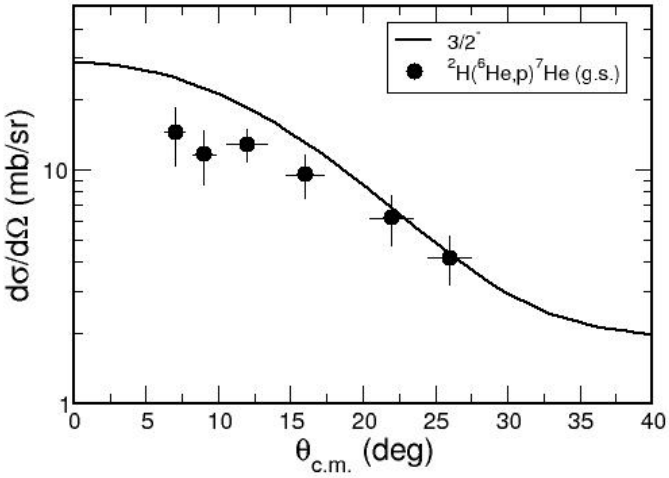

Fig. I-50. Angular distribution for the d(^{6}He,p)^{7}He ground-state transition.

g.2. Neutron Spectroscopic Factors in ^{9}Li from the d(^{8}Li,p)^{9}Li Reaction

(K. E. Rehm, J. P. Greene, D. J. Henderson, R. V. F. Janssens, C. L. Jiang, E. F. Moore, R. C. Pardo, S. Sinha, X. Tang, and R. B. Wiringa, D. Peterson, S. C. Pieper, G. Savard, J. P. Schiffer, A. H. Wuosmaa,* L. Jisonna,† M. Paul,‡ and R. E. Segel†)

Modern computational and theoretical techniques, such as the quantum Monte Carlo method[1] have made significant progress in the understanding of the structure of light nuclei. Many predicted properties are in good agreement with the measured values, however for many light nuclei data are unavailable due to the difficulty of populating these nuclei with the simple, well understood transfer reactions that have been used historically to probe nuclear structure. With unstable beams, it is now possible to carry out so-called "classical" nuclear physics measurements to study properties of light nuclei that had previously been inaccessible. One experimental property of the wave function of simple nuclear states is the neutron spectroscopic factor, for which the best probe is the (*d,p*) reaction. The *ab-initio* theoretical methods described[1] can be used to make first-principles predictions of the neutron spectroscopic factor.

We have studied the *d*(^{8}Li,*p*)^{9}Li reaction using a radioactive ^{8}Li beam to determine neutron spectroscopic factors in the nucleus ^{9}Li. In the *p* shell, (*d,p*) reactions have already been used extensively to determine single-

neutron spectroscopic factors for Li isotopes that can be produced with stable targets.[2]

In ^{9}Li, only 5 levels are known, with only the ground state assigned a firm spin-parity value of $3/2^-$.[3] To extend the available data for this nucleus, we have studied the inverse-kinematic reaction $d(^{8}\mathrm{Li},p)^{9}\mathrm{Li}$ using a radioactive ^{8}Li beam produced at the in-flight facility at the ATLAS accelerator at Argonne National Laboratory. The ^{8}Li beam was produced using the $d(^{7}\mathrm{Li},p)^{8}\mathrm{Li}$ reaction, with a ^{7}Li beam energy of 80 MeV, and an intensity of 50 pnA on the D_2 gas-cell production target. Due to the low Z and mass of the ^{8}Li secondary-beam particles, and the large difference in m/q between primary and secondary beams, the resulting ^{8}Li beam had very good transverse and longitudinal emittance properties and was very pure. This beam bombarded a 540 μg/cm^2 CD_2 foil target.

In an inverse kinematic (d,p) reaction, the protons of interest, emitted forward in the center-of-mass system, emerge at backward angles in the laboratory. These backward emitted protons were detected using an array of segmented annular silicon detectors, and the coincident ^{7,8,9}Li ions were detected and identified using an array of silicon EΔE telescopes at very forward angles. Figure I-51 shows a representative proton Q-value spectrum.[4]

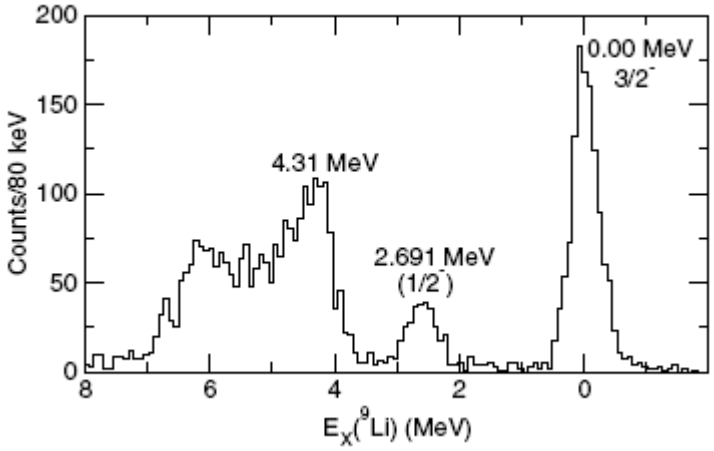

Fig. I-51. Excitation-energy spectrum for the $d(^{8}\mathrm{Li},p)^{9}\mathrm{Li}$ reaction.

Proton angular distributions for transitions to the ground, first- and second-excited states appear in Fig. I-52.[4] Also plotted in Fig. I-52 are curves representing the calculations of the transfer angular distribution using the code PTOLEMY which takes as input the calculated neutron spectroscopic factor for the $d(^{8}\mathrm{Li},p)^{9}\mathrm{Li}$ reaction. The solid and dashed curves represent the results from two different optical-model potential sets.[2] The data are in good agreement with the theory and show that the quantum Monte-Carlo calculations of neutron spectroscopic factors are reliable. The results also make it clear that measurements of simple, single-particle transfer reactions such as (d,p) can be carried out at the energies best suited to such measurements, between 6-10 MeV/ nucleon.

*Western Michigan University, †Northwestern University, ‡Hebrew University, Jerusalem, Israel.

[1]S. C. Pieper and R. B. Wiringa, Ann. Rev. Nucl. Part. Sci. **91**, 53 (2001); S. C. Pieper, K. Varga, and R. B. Wiringa, Phys. Rev. C **66**, 044310 (2002).
[2]J. P. Schiffer *et al*., Phys. Rev. **164**, 1274 (1967).
[3]P. G. Young and R. H. Stokes, Phys. Rev. C **4**, 1597 (1971); F. Ajzenberg-Selove *et al*., Phys. Rev. C **17**, 1283 (1978).
[4]A. H. Wuosmaa *et al.*, Phys. Rev. Lett. **94**, 082502 (2005).

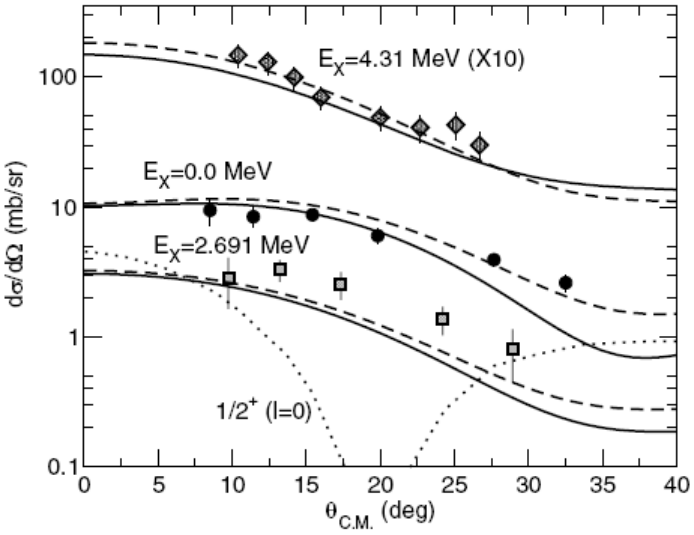

Fig. I-52. Angular distributions for three states in ^{9}Li, populated in the d(^{8}Li,p)^{9}Li reaction. Calculated angular distributions are discussed in the text.

g.3. Is the Nuclear Spin-Orbit Interaction Changing with Neutron Excess?

(J. P. Schiffer, S. J. Freeman,* C.-L. Jiang, P. D .Parker,† and K. E. Rehm)

The single-particle character of nuclei underlies much of our understanding of nuclear structure. The states formed by a proton outside the closed shell of 50 protons were studied with the (α,t) reaction on all the stable, even Sn isotopes two years ago to demonstrate that the spin-orbit splitting for the proton states was changing with neutron excess.[1] A closely related experiment, to obtain quantitative information on neutron single-particle states outside N = 82 with the (α,^{3}He) reaction, had been proposed, also to be carried out at the Yale ESTU tandem. Unfortunately, He beams were not available at Yale during the past year because of ion source problems and the experiments are planned for later in 2005 after the source has been replaced.

*University of Manchester, United Kingdom, †Yale University.

[1]J. P. Schiffer *et al*., Phys. Rev. Lett. **92**, 162501 (2004).

g.4. Hindrance of Heavy-Ion Fusion at Extreme Sub-Barrier Energies in Open-Shell Colliding Systems

(C. L. Jiang, K. E. Rehm, H. Esbensen, R. V. F. Janssens, B. B. Back, C. N. Davids, J. P. Greene, D. J. Henderson, C. J. Lister, R. C. Pardo, T. Pennington, D. Peterson, D. Seweryniak, B. Shumard, S. Sinha, X. D. Tang, I. Tanihata, S. Zhu, P. Collon,* S. Kurtz,* and M. Paul†)

Heavy-ion induced fusion reactions have been studied extensively for more than forty years, especially since the discovery of the sub-barrier enhancement phenomenon. Coupled-channels descriptions were shown to explain the phenomenon successfully. Recently, evidence was found for a strong hindrance of the fusion process at extreme sub-barrier energies, an effect for which there is no satisfactory explanation in present model calculations.[1-3] The aim of the present work is to further investigate the hindrance phenomenon by measuring fusion evaporation for the open-shell system ^{64}Ni + ^{100}Mo.

The experiment was performed with ^{64}Ni beams in the energy range of 196-262 MeV from the superconducting linear accelerator ATLAS at Argonne National Laboratory. The maximum beam current used was ~60 pnA. The high melting point of the target material, metallic molybdenum evaporated on a 40 μg/cm^{2} carbon

foil, prevented damage to the target by the relatively high beam current. The target thickness was constant during the experiment, as monitored with Si detectors. Thin targets with thicknesses of 8 or 18 μg/cm^2 were used in order to reduce the correction for target thickness in the energy regime of the steep fall off of the excitation function. The isotopic abundance of ^{100}Mo was 97.42%, with the remainder coming from ^{98}Mo (0.96%), ^{97}Mo (0.28%), ^{96}Mo (0.34%), ^{95}Mo (0.29%), ^{94}Mo (0.18%), and ^{92}Mo (0.53%). The selection of the beam and target combination excluded the possibility of background from fusion reactions coming from beam or target contaminants.[1] Two surface-barrier Si detectors, located at ±43° with respect to the beam direction, served as monitors. The absolute cross sections for fusion-evaporation were determined by measuring the elastic scattering in the monitors.

For most settings of the FMA, two charge states of the residues were collected simultaneously. For the energies E_{lab} = 260.5, 245.8, 209.1, 207.1 and 202.2 MeV, full charge state distributions were measured, while for most other energies, two FMA settings, *i.e.* four charge states were recorded. At the four lowest energies, only two charge states were measured. From the full charge state distributions, charge state fractions were determined for extrapolation to all other energies. The energy distributions and angular distributions of evaporation residues were calculated with the statistical code PACE.[4] Total angular distributions for fusion-evaporation have been measured in Ref. 5 for ^{64}Ni + ^{100}Mo. In order to check the PACE code, calculations were compared with these experimental angular distributions of Ref. 5 and good agreement was found as long as the total calculated angular distributions were taken as a weighted sum of the angular distributions of the different masses from our *m/q* measurements and folded with multiple scattering. Whereas in Ref. 5 rather thick targets were used, the corrections from multiple scattering are small in the present experiment. The transport efficiencies of the FMA were calculated with these angular distributions together with Monte Carlo simulations, using a modified version of the GIOS Code.[6] The large momentum acceptance, ±10%, and the large angular acceptance, $\theta_{lab} < 2.3°$, of the FMA result in a high detection efficiency for the residues. The detection of the residues has been described in another report.[7]

The fusion-fission cross sections for ^{64}Ni + ^{100}Mo have not been measured previously. They were, however, calculated in Ref. 5 with the code CASCADE.[8] Similar calculations with the same parameters were performed for the present experiment. Rather large uncertainties were given for the fusion-fission contributions resulting in somewhat larger errors for the total cross sections at the highest beam energies.

The experimental results for the total fusion cross sections, spanning eight orders of magnitude, are presented as a function of laboratory energy in Fig. I-53 (solid circles). The incident energies have been corrected for target thickness and for the steep energy dependence; these corrections are small because rather thin targets were used. For the lowest two energies no evaporation residue was observed. The results are shown as upper limits corresponding to one count in each case. The two earlier measurements[5,9] are also shown in Fig. I-53 as open circles and open squares, respectively. Statistical errors are smaller than the size of the symbols. The three measurements are generally in good agreement within the quoted uncertainties, except for the lowest energy point of Ref. 9.

Detailed coupled-channels calculations have been carried out. The ion-ion potential was parameterized as a Woods-Saxon well with a depth of V_0 = -82.9 MeV, diffuseness a = 0.686 fm, and nuclear radius R_N = 10.19 fm + ΔR. A value of ΔR = 0.21 fm was needed to reproduce the present data in the cross section region of 1 to 100 μb. The long-dashed curve in Fig. I-53 shows as a reference, the results obtained in a one-dimensional calculation, *i.e.*, without any couplings (with ΔR = 0.21 fm). The coupled-channels calculations exhibit essentially the same energy dependence (slope) as the one-dimensional calculation when the cross sections are small (<10 μb). The coupled-channels calculations are just shifted to lower energies relative to the one-dimensional calculation. In the present case the shift is about 7 MeV (for the same ΔR = 0.21 fm). This is a general feature of coupled-channels calculations and it is, therefore, very unlikely that any minor adjustment in the coupled-channels calculations would reproduce the steep fall off that the data exhibit at extreme sub-barrier energies. Thus, it appears that the fusion hindrance behavior, which now has been observed for many systems, is also present in the new data for ^{64}Ni + ^{100}Mo. This will be shown more convincingly in the following, where other representations of the fusion cross section are discussed.

The logarithmic derivative, $L(E) = d\ln(\sigma E)/dE$, originally introduced in Ref. 1, is shown in Fig. I-54a for the ^{64}Ni + ^{100}Mo system. The solid circles were obtained directly from two successive data points, whereas the stars were derived from least-squares fits to three

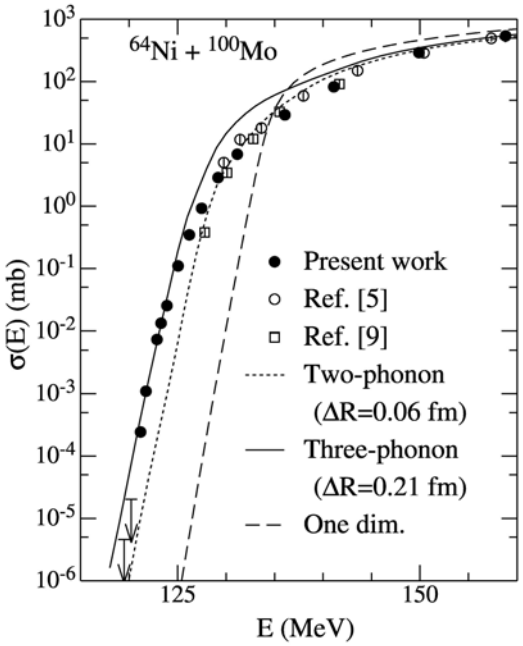

Fig. I-53. Fusion excitation function for ^{64}Ni + ^{100}Mo compared with several calculations described.

neighboring data points. The lower limit of the logarithmic derivative was derived from the upper limit on the cross section at E_{cm} = 120.2 MeV and the data point at E_{cm} = 121.2 MeV. The present data are compared to those of Refs. 5 and 9, which are represented by open circles and open squares in Fig. I-54a, respectively. Only two-point derivatives are shown for these data. The three-phonon coupled-channels and the one-dimensional barrier penetration calculations are shown as solid and long-dashed curves, respectively, while the thick solid, nearly horizontal line corresponds to the constant *S*-factor expression derived in Ref. 2. The present experimental results just reach the constant *S*-factor line, implying that the experimental data have reached a maximum value for the *S*-factor. The energy, E_s, representing the intersection between the experimental logarithmic derivatives and the constant *S*-factor line corresponds to a value of E_s = 120.6 MeV. The dotted line in Fig. I-54a is an extrapolation obtained under the assumption that the logarithmic derivative is a straight line near the crossing point. This method was first introduced in Ref. 3 in order to obtain the extrapolated values of E_s for the systems ^{58}Ni + ^{60}Ni and ^{58}Ni + ^{64}Ni. The calculated logarithmic derivatives are seen to saturate around L = 1.5 - 2 MeV^{-1} (or start to oscillate) below E_{cm} = 124 MeV, whereas the corresponding experimental values continue to grow with decreasing energies. This saturation behavior has already been noted in Refs. 1-3.

The *S*-factor representation for the ^{64}Ni + ^{100}Mo system is presented in Fig. I-54b. As the experimental logarithmic derivatives only just reach the constant *S*-factor curve, the *S*-factor maximum is not fully developed. Additional measurements would be required to clearly delineate the maximum in the *S*-factor. The dotted curve corresponds to the straight line extrapolation of the logarithmic derivative in Fig. I-54a. The two- and three-phonon calculations are shown in Fig. I-54b as dashed and solid curves, respectively. It is evident that coupled-channels calculations overpredict the fusion cross section at extreme sub-barrier energies.

The experimental fusion data involving Ni projectiles and compound nuclei in the A = 100-200 region have been summarized. For four systems, namely the ^{58}Ni + ^{58}Ni,[10] ^{64}Ni + ^{64}Ni,[3] ^{60}Ni + ^{89}Y[1] and the present ^{64}Ni + ^{100}Mo reactions, the cross sections have been measured to sufficiently low energies to determine the energy, E_s of the maximum of the *S*-factor representation. In addition, we have previously obtained the E_s values for the ^{58}Ni + ^{60}Ni[11] and ^{58}Ni + ^{64}Ni[12] systems[3] by extrapolation of the logarithmic derivative as explained below. Two additional systems, namely ^{58}Ni + ^{74}Ge[12] and ^{64}Ni + ^{74}Ge[12] from Ref. 13, have been measured down to levels close to where the *S*-factor maximum occurs. The

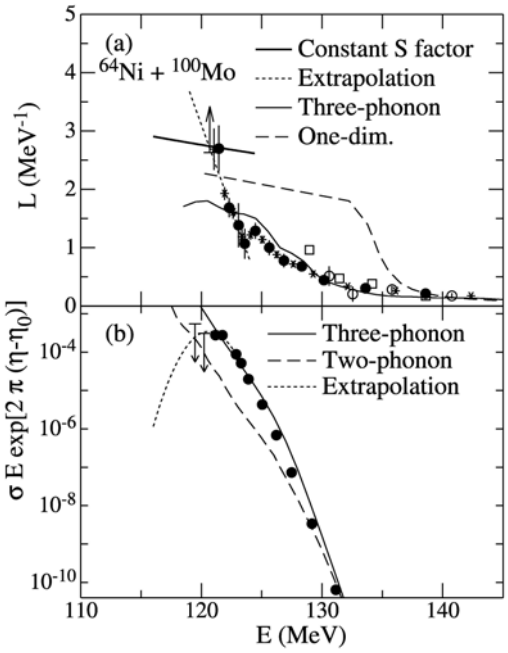

Fig. I-54. (a) Logarithmic derivative representation of the ^{64}Ni + ^{100}Mo fusion excitation function. The solid circles were obtained from two successive data points and stars were derived from least square fits to three neighboring data points. Included in are also the data from Ref. 5 (open circles) and Ref. 9 (open squares). (b) S-factor representation of the same data. Calculations are shown by curves in both panels. The extrapolation curve (dotted) shown in panel (b) was obtained from a straight line extrapolation of the logarithmic derivative representation in panel (a). A value of η_0 = 105.74 was used. See text for details.

location of the *S*-factor maximum was obtained by performing a small extrapolation of the logarithmic derivative to where it crosses the constant *S*-factor line. Because of the uncertainties inherent in these extrapolations, errors of 2% (~2 MeV) were assigned to the extrapolated E_s data, whereas an accuracy of 1% (~2 MeV) is obtained for the four systems where a maximum in the *S*-factor was observed.

The values of E_s are plotted as a function of the parameter $Z_1Z_2\mu^{1/2}$ in Fig. I-55 and compared to the empirical formula (solid curve)[2], which was obtained from a fit to all available fusion data involving stiff nuclei. Obviously, only two systems, ^{58}Ni + ^{58}Ni and ^{60}Ni + ^{89}Y follow the systematics; all other systems fall below the curve. Previously, it has been pointed out[3] that there is a rather compelling correlation between the stiffness of the interacting nuclei and the location of the *S*-factor maximum, E_s, relative to the empirical trend. The addition to the systematics of the data points for ^{64}Ni + ^{100}Mo and for the two Ni + Ge systems, which all involve soft nuclei, appears to corroborate this observation. Thus, for the ^{64}Ni + ^{100}Mo system, the value of E_s^{ref} predicted from the empirical formula is 134.5 MeV whereas the measured value of E_s = 120.6 MeV is only 90% of this value. The reason for this reduction is presumably that ^{64}Ni + ^{100}Mo should be viewed as an open-shell colliding system so that strong coupling effects broaden the effective barrier distribution and push the energy where the hindrance behavior occurs down to even lower energies.

The deviation of the measured or extrapolated values of E_s from the expected E_s^{ref} value, seen in Fig. I-55, thus appears to depend on the stiffness of the fusing nuclei. A quantitative relation between the stiffness and the deviation from E_s^{ref} is not yet known. As a first attempt, we associate the stiffness of a nucleus to its proximity to closed proton or neutron shells and define the number of "valence nucleons", N_{ph}, as the sum of particles and holes outside the nearest closed shells. Here, ^{64}Ni is considered to have four holes in the N = 40 neutron shell rather than eight particles outside N = 28. In Fig. I-56, the ratio E_s/E_s^{ref} is plotted as a function of this parameter. There is a general trend of decreasing values of E_s/E_s^{ref} with increasing values of N_{ph}. We observe that for the other systems not included in Fig. I-56, the data for E_{min} (upper limits) are not in contradiction with Figs. I-55 and I-56. It should be noted that all of the systems shown in Figs. I-55

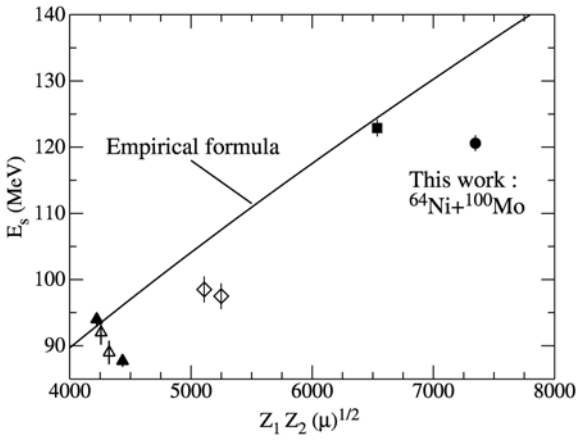

Fig. I-55. Plot of E_s vs. $Z_1Z_2\sqrt{\mu}$ for Ni bombarding different targets. Solid symbols correspond to systems for which the S-factor maximum is well determined: ^{64}Ni + ^{64}Ni, ^{60}Ni + ^{89}Y and ^{64}Ni + ^{100}Mo. Open symbols are associated with the extrapolations for the systems ^{58}Ni + ^{60}Ni, ^{58}Ni + ^{64}Ni, ^{58}Ni + ^{74}Ge and ^{64}Ni + ^{74}Ge. The triangles represent Ni + Ni, diamonds Ni + Ge, a square ^{60}Ni + ^{89}Y and a circle ^{64}Ni + ^{100}Mo, respectively.

and I-56 have rather large negative fusion Q-values. One may also compare the E_s-values to the height of the Coulomb barrier V_c (like obtained from the Bass prescription). The ratio E_s/E_s^{ref} exhibit a stronger dependency on the value of N_{ph} than that obtained for the ratio E_s/V_c indicating that the observed effect does not just depend on the change in the Coulomb barrier height with addition of neutrons to the interacting nuclei.

The above observations are all phenomenological in nature as there is at present no satisfactory understanding of the fusion hindrance at extreme sub-barrier energies. The data are most likely still insufficient to lead to the correct explanation. More precision sub-barrier fusion measurements are required to further explore which modifications in the theoretical models are relevant for a correct description of the phenomenon.

In conclusion, an interesting nuclear structure dependence of the fusion hindrance has been observed. The origin of this effect is still unknown. It occurs at relatively high excitation energies (for systems in Figs. I-55 and I-56, they are around E_{ex} ~ 30-40 MeV), where the natural width of compound levels is larger than their spacing. A lack of available final states thus appears to be ruled out as an explanation.

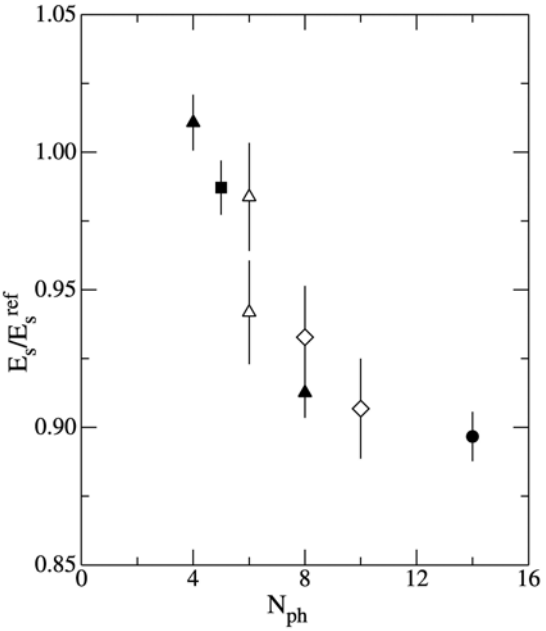

Fig. I-56. Plot of E_s/E_s^{ref} vs. N_{ph} , where N_{ph} is the total number of "valence nucleons" outside closed shells in the entrance channel. Symbols are defined in Fig. I-55.

---

*University of Notre Dame, †Hebrew University, Jerusalem, Israel.

[1]C. L. Jiang *et al*., Phys. Rev. Lett. **89**, 052701 (2002).
[2]C. L. Jiang, H. Esbensen, B. B. Back, R. V. F. Janssens, and K. E. Rehm, Phys. Rev. C **69**, 014604 (2004).
[3]C. L. Jiang *et al*., Phys. Rev. Lett. **93**, 012701 (2004).
[4]A. Gavron, Phys. Rev. C **21**, 230 (1980).
[5]K. E. Rehm, H. Esbensen, J. Gehring, B. Glagola, D. Henderson, W. Kutschera, M. Paul, F. Soramel, and A. H. Wuosmaa, Phys. Lett. **B317**, 31 (1993).
[6]C. L. Jiang and C. N. Davids, ANL Phys. Div. Annual Report **ANL-95/14**, 74 (1995).
[7]C. L. Jiang *et al*., submitted to Nucl. Instrum. Methods A.
[8]F. Pühlhofer, Nucl. Phys. **A280**, 267 (1977).
[9]M. L. Halbert, J. R. Beene, D. C. Hensley, K. Honkanen, T. M. Semkow, V. Abenante, D. G. Sarantites, and Z. Li, Phys. Rev. C **40**, 2558 (1989).
[10]M. Beckerman, J. Ball, H. Enge, M. Salomaa, A. Sperduto, S. Gazes, A. DiRienzo, and J. D. Molitois, Phys. Rev. C **23**, 1581 (1982).
[11]A. M. Stefanini *et al*., Phys. Rev. Lett. **74**, 864 (1995).
[12]M. Beckerman *et al*., Phys. Rev. C **25**, 837 (1982).

g.5. ^{58}Ni + ^{89}Y Fusion Hindrance at Extreme Sub-Barrier Energies

(C. L. Jiang, K. E. Rehm, H. Esbensen, B. B. Back, R. V. F. Janssens, J. P. Greene, D. J. Henderson, T. O. Pennington, D. Seweryniak, J. A. Caggiano,* P. Collon,† A. M. Heinz,‡ and I. Nishnaka§)

Fusion reactions between heavy ions have been studied extensively for a long time, especially since the discovery of the strong enhancement phenomenon at sub-barrier energies.[1] In most fusion-evaporation experiments carried out thus far, cross sections have been measured down to the 0.1 to 1 mb level, and coupled-channels calculations have been quite successful in reproducing the general trend of the measured yields.[2] It was recently found that heavy-ion fusion is often hindered at extreme sub-barrier energies,

where fusion cross sections are very small (say in the μb to nb region).[3-6] This phenomenon has not yet been explained in realistic model calculations.

The present work deals with the experimental results for the system ^{58}Ni + ^{89}Y and also reports on one of the experiences learned when the measured cross sections are very low; *i.e.* the influence of contaminants, either in the beam or in the target. We have previously measured the fusion evaporation excitation function for the ^{60}Ni + ^{89}Y system down to the 100 nb level and discussed the fusion hindrance phenomenon for this system in detail.[3-4] The excitation function obtained is reproduced in Fig. I-57 with open circles. It is seen that the cross section in this semi-logarithmic plot falls off increasing steeply as the energy becomes smaller.

The fusion-evaporation excitation function for the system ^{58}Ni + ^{89}Y was measured using the same technique applied in the ^{60}Ni + ^{89}Y experiment. The two measurements were performed at the Argonne superconducting linear accelerator ATLAS. The fusion-evaporation residues were identified and measured with the Fragment Mass Analyzer (FMA).[7] A mono-isotopic target of yttrium was used. More details can be found in Ref. 3. The measured fusion-evaporation excitation function for ^{58}Ni + ^{89}Y is shown in Fig. I-57 by solid circles, and the data are listed in Table I-3, together with the data for the ^{60}Ni + ^{89}Y system.

The lowest cross section measured for ^{58}Ni + ^{89}Y fusion is 0.070 ± 0.010 mb, much higher than what we obtained for the reaction ^{60}Ni + ^{89}Y, $<7.0 \times 10^{-5}$ mb. This is due to the fact that a small amount of ^{58}Fe contaminant was present in the ^{58}Ni beam. During the experiment, an ECR source was used and the subsequent beam transport system is not sufficient to separate all the isobars completely. For the ^{60}Ni beam, no other stable A = 60 isobar exists in nature, so the beam was pure. In contrast, for the ^{58}Ni beam, ^{58}Fe is a stable nucleus, with a natural isotopic abundance of 0.3%. A small amount of ^{58}Fe contamination could be present in the ^{58}Ni beam, and the fusion-evaporation residues from the reaction ^{58}Fe + ^{89}Y would not be identified as a background and would be counted as "real" products in the experiment. The exact amount of contamination in the beam depends on the operation of the ECR source. During the ^{58}Ni + ^{89}Y experiment, a component of ^{58}Fe, $< 10^{-4}$ was observed in the spectrum of the ECR source output, but the amount could not be determined precisely.

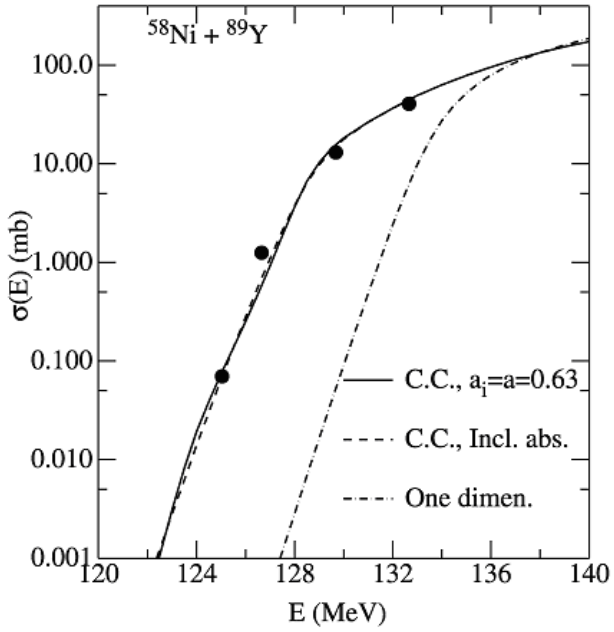

Fig. I-57. Fusion evaporation excitation functions for ^{58}Ni + ^{89}Y (solid circles) and ^{60}Ni + ^{89}Y (open squares) as function of the center-of-mass energy. Two open triangles are the measurements in which contributions from ^{58}Fe beam contaminations are not negligible.

Table I-3. Measured fusion evaporation cross sections for the systems ^{58}Ni + ^{89}Y and ^{60}Ni + ^{89}Y.

^{58}Ni + ^{89}Y			^{60}Ni + ^{89}Y		
$E_{c.m.}$ (MeV)	σ (mb)	Δσ (mb)	$E_{c.m.}$ (MeV)	σ (mb)	Δσ (mb)
157.4	140.3	21.0	136.3	109.7	16.5
144.6	203.0	30.5	131.2	28.7	4.3
132.7	40.6	6.1	129.7	11.5	1.7
129.7	13.0	2.0	127.9	5.5	0.82
126.7	1.25	0.19	126.4	2.1	0.32
125.0	0.070	.010	125.8	0.71	0.11
			124.9	0.42	.063
			124.2	0.094	.014
			123.5	0.030	.0049
			122.8	.0089	.0014
			122.1	.0016	3.9E-4
121.4	<7.0E-5				

The Coulomb barriers of ^{58}Ni + ^{89}Y and ^{58}Fe + ^{89}Y are 137.33 and 126.05 MeV (from the Bass model),[8] respectively. The sizeable difference in Coulomb barrier between the two systems translates in cross sections differing by orders of magnitude. The ratio of the cross sections for the two reactions is ~ 1000 at E = 125 MeV (indicated by the vertical dashed line in Fig. I-57). The contribution from ^{58}Fe induced fusion is much less than the uncertainty for the measurement at E = 125 MeV as this data point is in line with expectation (Fig. I-57). When the energy is even lower, however, the cross section for the reaction ^{58}Ni + ^{89}Y could easily decrease by orders of magnitude, while that for the reaction ^{58}Fe + ^{89}Y, would only decrease modestly. The ratio of the cross sections for the two reactions would, therefore, become greater than 10^4 at the lower energies. Thus, a minute amount of ^{58}Fe contamination in the ^{58}Ni beam could produce a significant contribution to the measured yield of evaporation residues and distort the measured data.

In order to test the above hypothesis, two extra measurements at lower energies than that of Table I-3 were carried out. It was found that the yields measured at these two energies were really abnormal, higher than expected. On the other hand, from PACE calculations[9] for the reaction ^{58}Ni + ^{89}Y, it is found that the ratio of the A = 144 to the A = 145 residues should decrease with decreasing energy. During the measurements, it was observed that this ratio does indeed decrease at the energies listed in Table I-3, but then starts to increase for these two additional energies. For the reaction ^{58}Fe + ^{89}Y, at the corresponding energies, residues of A = 144 are more abundant than those of A = 145. This observation points to the same conclusion, namely, that the contaminant, ^{58}Fe + ^{89}Y reaction starts to play a dominant role at energies lower than those of Table I-3. Thus data obtained at these two energies are not included in Table I-3 but included in Fig. I-57 as open triangles and this is the reason that our results for ^{58}Ni + ^{89}Y are restricted to 0.070 mb.

Our previous studies of the fusion hindrance phenomenon include the systems ^{64}Ni + ^{64}Ni and ^{64}Ni + ^{100}Mo, where ^{64}Ni was the beam.[5-6] It is conceivable that the ^{64}Ni beam was contaminated with ^{64}Zn. Because the element number Z is higher for ^{64}Zn than for ^{64}Ni, the corresponding Coulomb barrier is also higher, and the cross section for the ^{64}Zn induced fusion reactions will be smaller than that for ^{64}Ni induced reactions. The contribution from ^{64}Zn induced fusion reactions will, therefore, be negligible if the contamination of the ^{64}Ni beam is of the order of 10^{-4} or less.

In the following, we will try to estimate the hindrance phenomenon in the ^{58}Ni + ^{89}Y fusion reaction, although the excitation function was measured only in an energy range higher than the energy, Es where the hindrance is expected to set in.

Table I-4. Structure input for the low-lying states in ^{58}Ni. The B(Eλ)-values for the quadrupole transitions are from Ref. 10, and the octupole transitions are from Ref. 11.

Nucleus	λ^{π}	E_x (MeV)	B(Eλ) (b^{λ})	β_{λ}^{C}	β_{λ}^{N}
^{58}Ni	2^+	1.454	680	0.181	0.208
	2ph(4^+)	2.908		0.181	0.208
	3-	4.475	18600[11]	0.204	0.209

We performed detailed coupled-channels calculations (C.C.) for ^{58}Ni + ^{89}Y fusion. These are similar to those reported for ^{60}Ni + ^{89}Y.[4] The nuclear structure input for ^{58}Ni is given in Table I-4, while the input for ^{89}Y is the same.[4] The calculated results are shown in Figs. I-58 and I-59, where they are compared with the data. The solid curve in Fig. I-58 is based on a real ion-ion potential, with the same parameters.[4] Fusion is simulated by in-going-wave boundary conditions and the fusion cross section is obtained from the in-going flux inside the Coulomb barrier, near the local minimum of the interaction potential. The dashed curve in Fig. I-58 is based on a similar calculation, but it includes an additional short-ranged imaginary potential. Fusion is then obtained as the sum of the absorbed and in-going fluxes. These two methods produce almost identical excitation functions, but there are some differences which can be seen more clearly in the logarithmic derivative representation discussed below. The dashed-dotted curve shows the results of one-dimensional penetration calculations based on the same ion-ion potential.

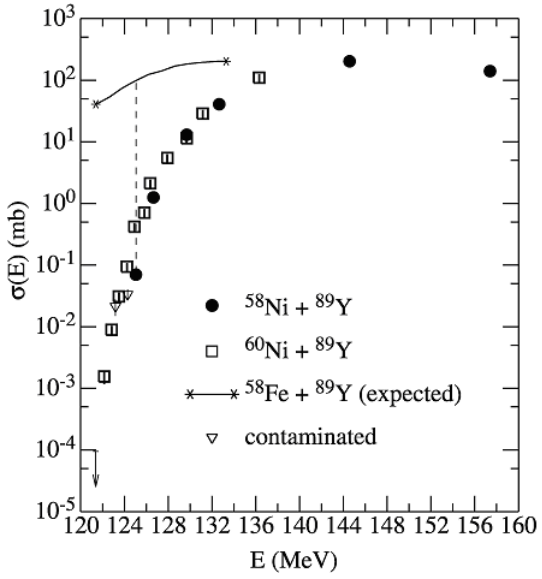

Fig. I-58. Fusion evaporation excitation function for ^{58}Ni + ^{89}Y (solid circles) and model calculations. The solid curve is the result of C.C. calculations based on a real ion-ion potential. The dashed curve includes also an additional short-ranged imaginary potential. The dashed-dotted curve represents one dimensional penetration calculations.

A new recipe for the ion-ion potential was introduced,[4] which modifies the ion-interaction for r < R (here r is the distance between ^{58}Ni and ^{89}Y ions, and R, the radius parameter of the potential), with a larger diffuseness a_i, but keeps the interaction unchanged for r > R (with a diffuseness a). The two interactions match up at r = R with a continuous derivative. Calculations based on this recipe are shown in Fig. I-59 and are compared with the original one (solid curve). The dotted and dashed curves are both from $a_i = 2a$ calculations, but with and without the imaginary potential, respectively. It appears that the $a_i = 2a$

calculations produce better fits to the data than the original $a_i = a$ ones.

The logarithmic derivative, L(E) = dln(Eσ)/dE, and the S-factor, S(E) representations for the reaction ^{58}Ni + ^{89}Y are given in Figs. I-60a and I-60b, respectively. The solid circles and triangles in Fig. I-60a show the values of L(E) obtained from two successive data points and from least square fits to three neighboring data points, respectively.

In the case of ^{60}Ni + ^{89}Y and other stiff ones, the experimental L(E) data increase with decreasing energy[4] and pass through the constant S-factor curves. For ^{58}Ni + ^{89}Y, the experimental L(E) curve does not yet reach the constant S-factor curve.[4] An extrapolation line (solid line) can be obtained using the method developed.[5] This line intersects the constant S-factor curve (dashed-dotted line) at 124.1 ± 2 MeV. The energy of this crossing point is the location E_s of the maximum in the *S*-factor curve. The experimental values of S(E) are presented in Fig. I-60b by the solid circles. The open circles show the values[3,4] for the reaction ^{60}Ni + ^{89}Y. The solid curve for ^{58}Ni + ^{89}Y is obtained from the linear extrapolation of L(E) shown in Fig. I-60a. It exhibits a maximum S-factor at the energy E_s = 124.1 ± 2 MeV, as determined above. As references, data from the two contaminated measurements are included in Fig. I-60a by corresponding open symbols.

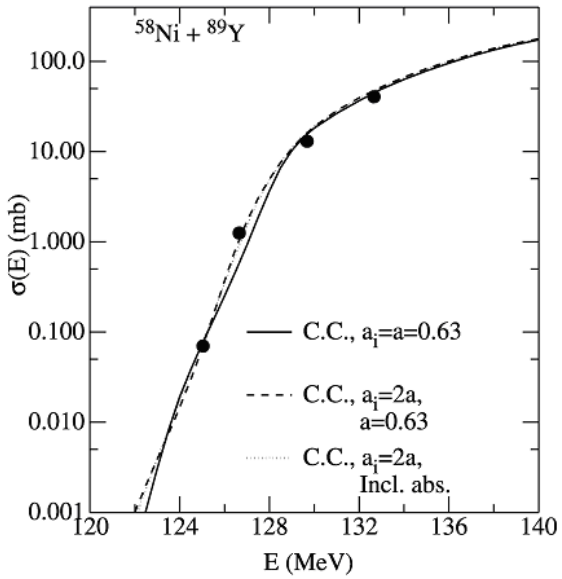

Fig. I-59. Fusion evaporation excitation function for ^{58}Ni + ^{89}Y (solid circles) and model calculations. The solid curve is the same as in Fig. I-58; the dotted one corresponds to $a_i = 2a$ with an imaginary potential, dashed, $a_i = 2a$ without an imaginary potential. See text for details.

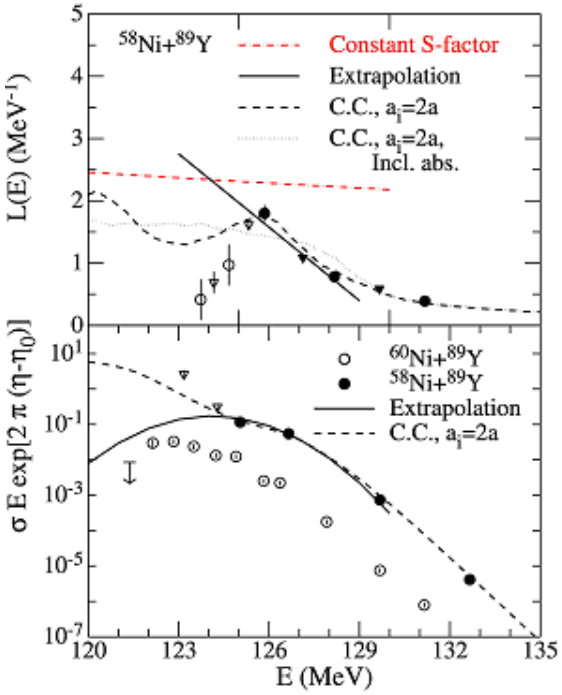

Fig. I-60. Logarithmic derivative representations (a) and S-factor representations (b) for the systems $^{58}Ni + ^{89}Y$ and $^{60}Ni + ^{89}Y$. Model calculations are included. Open symbols in (a) and open triangles in (b) are data from contaminated measurements. See text for details.

The results from some of the C.C. calculations are also included in Fig. I-60. The calculations for $a_i = 2a$ without the imaginary potential display an oscillatory behavior at the lowest energies (dashed curve), but these amplitude of the oscillations is strongly reduced when an imaginary potential is employed in the calculations (dotted curve). Similar behaviors occur for the two calculations displayed in Fig. I-58. The logarithmic derivatives of the C.C. calculations shown in Fig. I-60a are seen to saturate at values that are below the constant S-factor curve. Consequently, the associated S-factors do not exhibit a maximum.

In the systematic study reported[4] it was shown that the energy E_s, where the maximum S-factor occurs, can be described rather well for stiff, closed-shell colliding systems by the empirical formula

$$E_s^{ref} = 0.356\,(Z_1Z_2\mu^{1/2})^{2/3}\,(\text{MeV}), \qquad (1)$$

where $\mu = A_1A_2/(A_1+A_2)$. For softer systems, this formula provides an upper limit for the energy where the *S*-factor has its maximum. The E_s value for $^{58}Ni + ^{89}Y$ obtained above, with an uncertainty of 2 MeV, is compared in Fig. I-61 with the empirical formula of Eq. (1). The agreement between data the empirical formula is quite satisfactory. This was expected because the system $^{58}Ni + ^{89}Y$ belongs to a category of stiff heavy-ion systems. It is, therefore, very plausible that the fusion of $^{58}Ni + ^{89}Y$ is actually hindered at low energies.

An abnormal behavior of the fusion cross section may also occur at extreme sub-barrier energies, when heavy isotopic contaminants are present in a target. For isotopic targets, like ^{A}Ni, ^{A}Zr, ^{A}Mo, ^{A}Sm, etc., there are often several other isotopic components, ranging from 0.1% to several percents in any isotopically enriched targets. If one measures the excitation function for a light-isotopic target, the contributions from a heavy-isotopic contamination can become a serious problem at extreme sub-barrier energies *i.e.*, at very low cross sections. The reason is that the center of mass energy is higher for heavier isotopes and fusion cross sections are thus usually larger for the heavier systems at the same beam energy. Hence, even a very small contamination is likely to show up at very low energies. On the other hand, the isotopic contamination of the target would not be such a serious problem if one wants to measure fusion reaction with the heaviest isotope. This is one of the reasons why ^{64}Ni and ^{100}Mo targets were selected in our studies of fusion hindrance at extreme sub-barrier energies.[5,6]

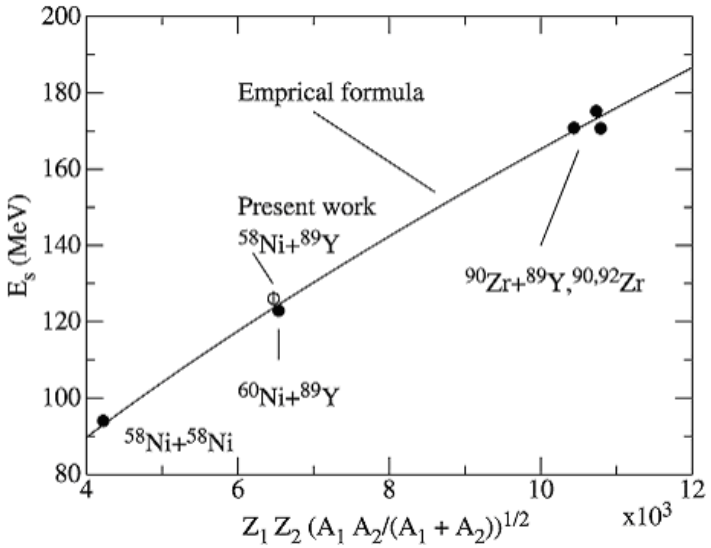

Fig. I-61. Plot of Es vs. $Z_1Z_2\mu^{1/2}$ for some stiff colliding systems. The open circle is for the present work, ^{58}Ni + ^{89}Y. Solid symbols are for other well determined stiff systems. Solid curve is from Eq. (1).

In the literature, one can find many measurements that use light-isotope targets, and some of the excitation functions do exhibit an abnormal behavior at extreme sub-barrier energies, which could perhaps be caused by the isotopic contamination mechanism discussed above. The abnormal behavior may not be seen so clearly in a plot of the excitation function, but it could probably be seen more clearly in the other representations, *i.e.* in terms of L(E) or S(E).

In summary, the influence of isobaric contamination of the beam, and/or isotopic contamination in the target, may introduce a serious problem in measure-ments of fusion-evaporation residues at extreme sub-barrier energies. The fusion hindrance at extreme sub-barrier energies was extracted for the reaction ^{58}Ni + ^{89}Y, and it was found to be consistent with the systematics obtained for stiff systems.

---

*TRIUMF, Vancouver, British Columbia, †University of Notre Dame, ‡Yale University, §JAERI, Japan.

[1]M. Beckerman, Physics Report **129**, 145 (1985); M. Beckerman, Rep. Prog. Phys. **51**, 1047 (1988); R. Vandenbosch, Annu. Rev. Nucl. Part. Sci. **42**, 447 (1992); A. B. Balantekin and N. Takigawa, Rev. Mod. Phys. **70**, 77 (1998); M. Dasgupta, D. J. Hinde, N. Rowley, and A. M. Stefanini, Annu. Rev. Nucl. Part. Sci. **48**, 401 (1998).
[2]K. Hagino and N. Takigawa, Phys. Rev. C **55**, 276 (1997).
[3]C. L. Jiang *et al*., Phys. Rev. Lett. **89**, 052701 (2002).
[4]C. L. Jiang, H. Esbensen, B. B. Back, R. V. F. Janssens, and K. E. Rehm, Phys. Rev. C. **69**, 014604 (2004).
[5]C. L. Jiang *et al*., Phys. Rev. Lett. **93**, 012701 (2004).
[6]C. L. Jiang *et al*., Phys. Rev. C **71**, 044613 (2005).
[7]C. N. Davids and J. Larson, Nucl. Instrum. Methods **B40/41**, 1224 (1989); **A345**, 528 (1994).
[8]R. Bass, Nucl. Phys. **A231**, 45 (1974).
[9]A. Gavron, Phys. Rev. C **21**, 230 (1980).
[10]J. Charbonneau *et al.,* Bull. Am. Phys. Soc. (1971).
[11]M. A. Duguay *et al.*, Phys. Rev. **12**, 1677 (1967).

g.6. Hindrance of Heavy-Ion Fusion at Extreme Sub-Barrier Energies for a Small Q-Value System ^{28}Si + ^{64}Ni

(C. L. Jiang, K. E. Rehm, B. B. Back, H. Esbensen, R. V. F. Janssens, C. N. Davids, J. P. Greene, D. J. Henderson, L. Jisonna, C. J. Lister, M. Notani, R. Pardo, D. Peterson, D. Seweryniak, B. Shumard, X. D. Tang, I. Tanihata, X. F. Wang, S. F. Zhu, P. Collon,* S. Kurtz,* and M. Paul†)

An unexpected hindrance of heavy-ion fusion at extreme sub-barrier energies has been observed in experiments performed at ATLAS.[1-4] It was observed that the excitation functions of some heavy-ion fusion reactions exhibit an abrupt decrease in cross section at extreme sub-barrier energies. This decrease cannot be described by present model calculations.

In all measurements of the hindrance phenomenon investigated thus far, the Q-value for heavy-ion fusion is rather negative, Q < -36 MeV. As a result it is inevitable that the S-factor must reach a maximum at sufficiently low beam energies as the final state phase space disappears as the centre-of-mass energy, E approaches -Q (see Ref. 2 for a detailed discussion). This behavior is different from that seen in light-ion or light heavy-ion fusion reactions, *e.g.*, ^{16}O + ^{16}O[5], where $S(E)$ is a rather flat function at very low energies.

In order to further explore this issue, we have measured the fusion-evaporation excitation function for the system ^{28}Si + ^{64}Ni down to 30 nb. This system has a rather small negative fusion Q-value (Q = -1.78 MeV). The experiment was performed with ^{28}Si beams in the energy range of 63 - 95 MeV from the superconducting linear accelerator ATLAS at Argonne National Laboratory. The maximum beam current used was ~100 pnA. The high melting point of the target material, metallic Nickel evaporated on a 40 μg/cm^2 carbon foil, prevented damage to the target by the relatively high beam current. Thin targets with thicknesses of about 15 μg/cm^2 were used in order to reduce the correction for target thickness in the energy regime of steep fall off of the excitation function. The isotopic abundance of ^{64}Ni was 98.02%, with the remainder coming from ^{58}Ni (0.97%), ^{60}Ni (0.57%), ^{61}Ni (0.05%) and ^{62}Ni (0.39%). The selection of the beam and target combination excluded the possibility of background from fusion reactions coming from beam or target contaminants.[1] Two surface-barrier Si detectors, located at ±43° with respect to the beam direction, served as monitors. The absolute cross sections for fusion-evaporation were determined by using elastic scattering measured with the monitors.

The evaporation residues were analyzed with the Fragment Mass Analyzer (FMA)[6] at 0°, which has been upgraded with the installation of a split-anode in the first electric-dipole.[7] The background, originating mostly from scattered beam, was greatly suppressed after this upgrade. The evaporation residues were detected and identified with a focal-plane detector with the configuration PGAC-TIC-PGAC-TIC-PGAC-IC.[8] Here, the symbols PGAC stand for x-y position sensitive parallel grid avalanche counters, TIC for transmission ionization chambers and IC for a large volume multi-anode ionization chamber. The first PGAC was mounted at the horizontal (x-direction) focal-plane of the FMA. Only one charge state can be measured at each FMA setting. Full charge state distributions were measured at five energies. Three to five charge states were measured at five intermediate energies and one charge state was measured for the lowest six energies. These data are sufficient to determine with the desired accuracy the charge state fractions of the detected evaporation residues.

The angular distributions of evaporation residues were obtained by measuring their velocity distributions. This method was developed previously at Argonne.[9] Assuming an isotropic emission of particles from the fused system, which is a rather good assumption at low energies, the velocity-distribution of the evaporation residues is also isotropic in the center-of-mass system. A measurement of the velocity distribution in the laboratory system at zero degree therefore yields the complete information about the velocity distribution, also in the transverse direction, which is required to compute the angular distribution and the evaporation residue cross sections.

Because the quantity

$$\frac{1}{v^2}\frac{d^2\sigma}{d\Omega dv} \qquad (1)$$

is invariant under the transformation between the laboratory system and the center-of-mass system, one obtains

$$\frac{d^2\sigma}{d\Omega_{cm}dv_{cm}}(\theta_{cm}=0^\circ)=\frac{v_{cm}^2}{v_{lab}^2}\frac{d^2\sigma}{d\Omega_{lab}dv_{lab}}(\theta_{lab}=0^\circ). \qquad (2)$$

Since $d^2\sigma/d\Omega_{cm}dv_{cm}$ is independent on the angle we obtain the total cross section σ_{total} following

$$\sigma_{total} = \int\int \frac{d^2\sigma}{d\Omega_{cm}dv_{cm}} d\Omega_{cm}dv_{cm} = 4\pi \int \frac{d\sigma}{dv_{cm}} dv_{cm}, \quad (3)$$

where v_{lab} and v_{cm} are the velocity magnitudes of the evaporation residues in the laboratory and centre-of-mass systems, respectively, and $v_{lab} = v_{cm} + v_0$ at 0° (v_0 is the centroid of the velocity distribution of the center of mass in the laboratory system).

Moreover one can get the angular distribution in the laboratory system also by using the following equations:

$$\frac{d^2\sigma}{d\Omega_{lab}dv_{lab}}(\theta_{lab}) = \frac{v_{lab}^2}{v_{cm}^2} \frac{d^2\sigma}{d\Omega_{cm}dv_{cm}}(\theta_{cm} = 0^\circ) = \frac{v_{lab}^2}{v_{lab}^2 + v_0^2 \quad 2v_{lab}v_0 cos(\theta_{lab})} \frac{d^2\sigma}{d\Omega_{cm}} dv_{cm}(\theta_{cm} = 0^\circ). \quad (4)$$

$$\frac{d\sigma}{d\Omega_{lab}} = \int \frac{d^2\sigma}{d\Omega_{lab}dv_{lab}}(\theta_{lab}) d\Omega_{lab}, \quad (5)$$

where $\vec{v}_{lab} = \vec{v}_{cm} - \vec{v}_0$.

Two methods have been used to measure the velocity spectra, the flight time from the target to the $PGAC_1$, or the flight time between $PGAC_1$ and $PGAC_3$. The FMA efficiency was calculated by using these deduced angular distributions.

The primary experimental result of the excitation function (down to about 30 nb) is show in Fig. I-62. This system has been measured previously by the Legnaro group[10] down to a cross section of 41 μb. In the near barrier region the two measurements agree well within experimental uncertainties. There is an energy shift, $\Delta E_{lab} \sim 1.2$ MeV between these two experiments. This situation is rather similar to experiments for the fusion system ^{64}Ni + ^{64}Ni, where an energy shift, $\Delta E_{lab} \sim 1.5$ MeV was observed between Argonne's measurement and Ref. 11.

Coupled channel calculations fitted to the Legnaro data[12] are plotted in Fig. I-62 by the solid line (with an energy shift of 0.8 MeV). Obviously, they over predict the present cross sections at extreme sub-barrier energies.

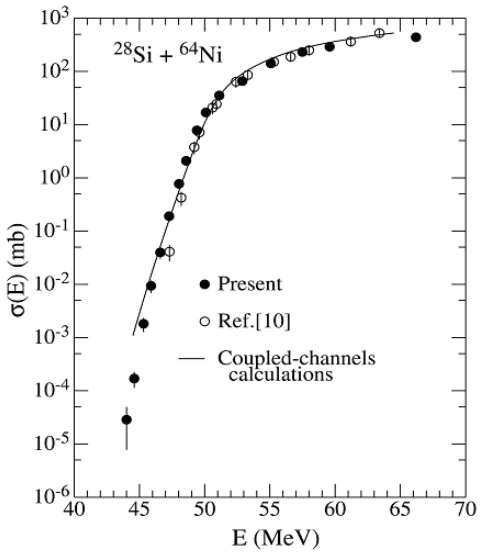

Fig. I-62. Excitation function for ^{28}Si + ^{64}Ni. Solid circles are our preliminary results. Open circles are taken from Ref. 10.

The deduced logarithmic derivatives $L(E)$ and the S-factor are shown in Fig. I-63. In Fig. I-63a the solid line is the constant S-factor expression that was derived in Ref. 2. The dotted line is a linear fit to the low-energy experimental $L(E)$ data. The crossing point of these two lines determines the location of the maximum of S-factor. There is a clear maximum in the S-factor (see Fig. I-63b), which cannot be reproduced by the

coupled-channels calculations (long-dashed curve, shifted by 0.8 MeV). It thus seems that the fusion hindrance behavior also exists for the system ^{28}Si + ^{64}Ni. The dotted curve in Fig. I-63b was obtained from the extrapolation line in Fig. I-63a. Data analysis is still in progress.

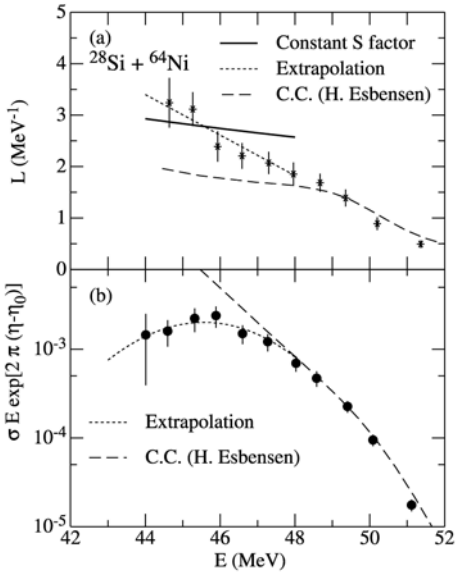

Fig. I-63. (a) The logarithmic derivative L(E) = d(ln σE)/dE, plotted as the function of center-of-mass energy E for ^{28}Si + ^{64}Ni. Stars are obtained from least-squares fits to three data points. (b) The S-factor S(E) = σEexp(2 πη), plotted as function of center-of-mass energy E. Solid circles are experimental results. The solid curve corresponds to a constant S-factor.[2] Long-dashed curves are coupled-channels calculations and dotted curves are extrapolation results.

---

*University of Notre Dame, †Hebrew University, Jerusalem, Israel.

[1]C. L. Jiang *et al*., Phys. Rev. Lett. **89**, 052701 (2002).
[2]C. L. Jiang *et al.,* Phys. Rev. C **69**, 014604 (2004).
[3]C. L. Jiang *et al.,* Phys. Rev. Lett. **93**, 012701 (2004).
[4]C. L. Jiang *et al.,* Phys. Rev. C **71**, 044613 (2005).
[5]R. G. Stokstadt *et al.,* Phys. Rev. Lett. **37**, 888 (1976).
[6]C. N. Davids and J. D. Larson, Nucl. Instrum. Methods **B40/41**, 1224 (1989); C. N. Davids, B. B. Back, K. Bindra, D. J. Henderson, W. Kutschera, T. Lauritsen, Y. Nagame, P. Sugathan, A. V. Ramayya, and W. B. Walters, Nucl. Instrum. Methods **B70**, 358 (1992).
[7]C. N. Davids, ANL Phys. Div. Annual Report **ANL-03/23**, 104 (2003).
[8]C. L. Jiang *et al.,* submitted to Nucl. Instrum. Methods A.
[9]C. L. Jiang *et al.,* ANL Phys. Div. Annual Report **ANL-97/14**, 55 (1997).
[10]A. M. Stefanini *et al.*, Nucl. Phys. **456**, 509 (1986).
[11]D. Ackermann *et al*., Nucl. Phys. **A609**, 91 (1996).
[12]H. Esbensen, private communication.